EX3/2

ENERGY AND PARTICLE CONTROL CHARACTERISTICS OF THE ASDEX UPGRADE 'LYRA' DIVERTOR

M. Kaufmann, H-S. Bosch, A. Herrmann, A. Kallenbach, K. Borrass, A. Carlson, D. Coster, J.C. Fuchs, J. Gafert, K. Lackner, J. Neuhauser, R. Schneider, J. Schweinzer, W. Suttrop, W. Ullrich, U. Wenzel, and ASDEX Upgrade team

Max-Planck-Institut für Plasmaphysik, EURATOM-IPP Association, Garching und Berlin, Germany

Abstract

In 1997 the new 'LYRA' divertor went into operation at ASDEX Upgrade and the neutral beam heating power was increased to 20 MW by installation of a second injector. This leads to the relatively high value of P/R of 12 MW/m. It has been shown that the ASDEX Upgrade LYRA divertor is capable of handling such high heating powers. Measurements presented in this paper reveal a reduction of the maximum heat flux in the LYRA divertor by more than a factor of two compared to the open Divertor I. This reduction is caused by radiative losses inside the divertor region. Carbon radiation cools the divertor plasma down to a few eV where hydrogen radiation losses become significant. They are increased due to an effective reflection of neutrals into the hot separatrix region. B2-Eirene modelling of the performed experiments supports the experimental findings and refines the understanding of loss processes in the divertor region.

1. INTRODUCTION

The width of the scrape-off layer (SOL) does not necessarily increase in proportion to the size of the device. This poses severe problems for the power exhaust in a fusion reactor. If we take ITER as described in the final design report (FDR) [1], a power flow across the separatrix in the order of 100 to 150 MW might be needed to stay in the H-mode [2]. A major fraction of this power has to be radiated to side walls before reaching the divertor target plates in order to limit the maximum deposited power density to technically feasible values below 10 MW/m^2. The ITER FDR reference divertor [1] has been designed according to these requirements, but the basic ideas are still to be confirmed by experiments.

Because of its geometrical similarity, the available heating power and the extensive diagnostics, the ASDEX Upgrade divertor tokamak plays a key role in this ITER R&D programme. In order to investigate the impact of the geometry on the divertor performance, the relatively open divertor configuration (Div I) has been replaced recently by a deeper, rather tightly baffled divertor with strongly inclined and inverted target plates (Div II, or 'LYRA' divertor), resembling the present ITER divertor design. In parallel to the divertor reconstruction, the neutral injection heating power was doubled from 10 to 20 MW by adding a second injector box. In this paper, we concentrate on the power handling and the helium exhaust capability of the new LYRA divertor.

2. EXPERIMENTAL SETUP OF ASDEX UPGRADE

2.1. The ASDEX Upgrade LYRA-Divertor

The old Div I configuration (Fig. 1, left part) in ASDEX Upgrade was characterized by flat horizontal divertor plates, where the outer target plate was put close to the X-point to benefit from the large flux expansion in that region. The target material was fine grain graphite. It had a relatively open divertor chamber with a small pumping baffle in the outer divertor, which nevertheless was quite important for good particle exhaust.

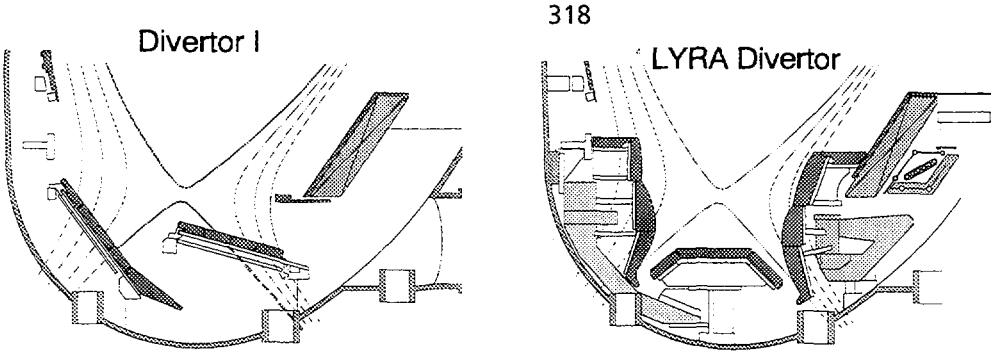

Figure 1: Poloidal cross-section of ASDEX Upgrade with Div I (left) and Div II in the LYRA configuration being operational since 1997 (right).

The new, fairly closed, LYRA divertor [3] (Fig. 1, right part) was designed to test the physics of the proposed ITER divertor, in particular the exhaust of power and particles consistent with good core confinement. Additionally, ASDEX Upgrade needed a hardened divertor to be able to operate at increased heating power. Div II is relatively deep and well baffled towards the main chamber. Based on experimental observations in Div I and on modelling calculations, the target plates and the roof baffle were shaped to improve the detachment properties and to reduce the target heat flux especially close to the separatrix. The constructive measure taken to increase the power handling capability of the LYRA divertor is the use of toroidally tilted carbon fibre composite (CFC) targets for the strike point modules to avoid leading edges. The power flow for a 5 s pulse is limited by the heat capacity of the target and the maximum tolerable surface temperature to about 9 MW/m^2.

2.2. Pumping, Heating and Diagnostics

For the LYRA divertor experimental phase the existing pumping system, consisting of 14 turbomolecular pumps with 10 m^3/s total pumping efficiency, was improved by adding a cryopump with 100 m^3/s nominal pumping speed. The cool-down of the cryopump to liquid He temperature (4.2 K) reduces the vacuum vessel pressure by almost a factor of 10 and allows a better control of the edge density during plasma discharges.

The total neutral beam heating (NBI) power has been doubled by installing a second injector reaching a total of 14 MW in H^0 (55 keV) or 20 MW in D^0 (60 keV). The new divertor geometry and the installation of the second injector required the redesign and adaption of existing diagnostics as well as the installation of new systems. Effort was made to get information as comprehensive as possible about the divertor plasma and the plasma target interaction as a prerequisite to understand the interplay of the various loss mechanisms which finally determine the heat flux to the divertor.

3. EXPERIMENTAL RESULTS

3.1. Experimental Parameters

To obtain a reference point for experimental parameter variations and modelling, a reference discharge was defined and repeated several times, allowing the collection of data with different settings of particular diagnostics and the demonstration of the reproducibility of the results. The heating power was chosen to be 15 MW neutral beam injection, resulting in a high value of the parameter $P_{heat}/R_0 = 9$ MW/m [4]. The electron density was set to a medium value $\bar{n}_e/n_e^{Greenwald} = 0.5$, corresponding to the natural H-mode density with no gas puffing and no cryopumping. The selected density value together with the restriction to 15 MW heating power results in good plasma performance ($H^{ITER89P} \leq 1.8$, $\beta_N \leq 2.6$) just below the onset of neoclassical tearing modes [5], which would distort the SOL observations. A power scan from 2.5 to 15 MW in the type-I ELMy H-mode regime is used to investigate the dependence of the divertor radiation on input power, comparisons between Div I and Div II are done for the intermediate power

level of 5 MW. The variation of the plasma current from 1 to 0.4 MA demonstrates the influence of SOL transport for the divertor load. All data presented in this paper are obtained without impurity seeding.

3.2. Radiation losses

3.2.1. Radiation pattern

Radiation from ASDEX Upgrade plasmas is measured routinely and the radiation patterns are calculated using anisotropic diffusion model tomography [6]. Fractional radiative powers P_{rad}/P_{heat} for the divertor and the main chamber are shown in Fig. 2 versus the heating power for various confinement regimes. No pronounced dependence on the heating power is seen, except a slight decrease of the fractional divertor radiation with P_{heat} for Div II. Radiation from the divertor (i.e. all radiation below a virtual horizontal line through the X-point) typically amounts to about 40% of the input power for Div II. Significantly lower values are seen for low plasma currents, a fact which is attributed to the increased SOL transport in these cases which diminishes the power input into the narrow divertor region.

In Div I the divertor radiation fraction was only about 20%. The main chamber radiative fraction is comparable for both divertor configurations.

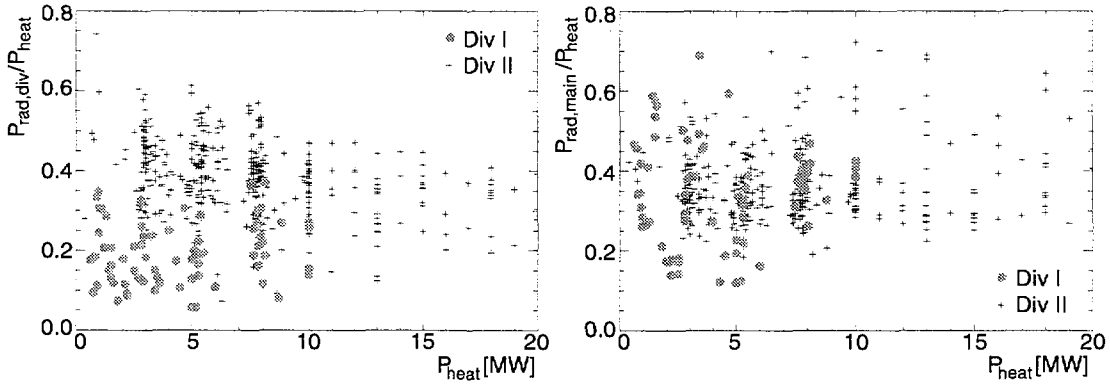

Figure 2: Radiated power normalized to the heating power a) (left) in the divertor and b) (right) in the main chamber. The data set includes ohmic, L-mode, and H-mode discharges.

3.2.2. Radiation on divertor plates

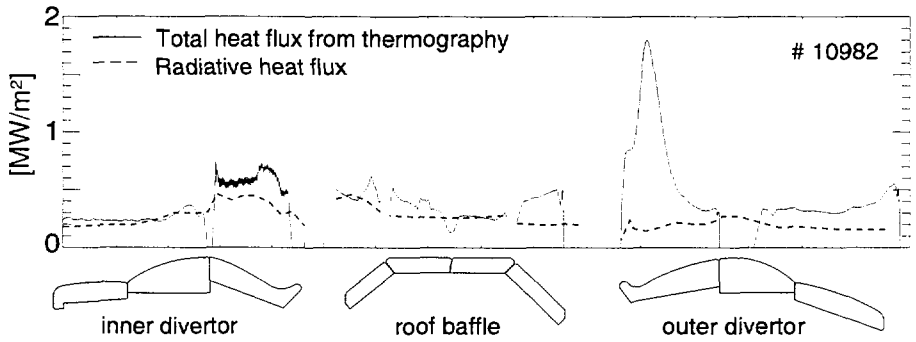

Figure 3: Total heat flux to the divertor plates measured by thermography and radiative heat flux calculated from the reconstructed radiation pattern for the reference discharge.

The major fraction of power radiated in the divertor region is absorbed by the divertor structure due to the closed geometry of the LYRA and is measured both by bolometry and thermography. This radiative heat flux to the divertor targets is calculated from the radiation pattern and compared to the total heat flux as measured by thermography [7], as shown in Fig. 3. It is obvious that the thermography has to be corrected for the radiative heat flux to obtain that part which is transferred by the plasma to the divertor

(plasma heat flux). Except at the outer strike point module the total heat flux is dominated by radiation. The plasma heat flux to the inner strike point is underestimated by the fast thermography system which observes a shadowed region of the tilted strike point modules.

Figure 4 shows the power balance for the reference conditions including 2 heating power plateaus of 5 and 15 MW, with the radiation correction of the thermographic measurement included. The power balance is fulfilled very well (within 10 %), the small amount of missing power is attributed to fast particle losses and the underestimation of the inner divertor load.

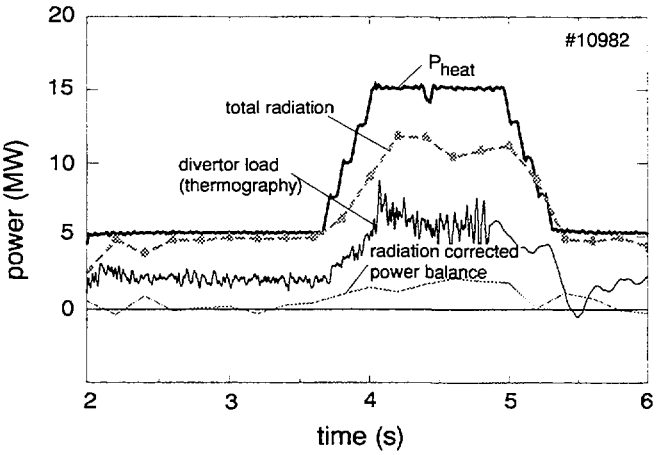

Figure 4: Power balance for the reference discharge with two heating power plateaus at 5 and 15 MW. $D^0 \rightarrow D^+$ NBI, $I_p = 1$ MA, $B_t = -2.5T$, $q_{95} = 4$.

3.3. Divertor target load

The divertor load in ASDEX Upgrade is measured by 3 thermography systems [7]. Heat flux profiles across the outer strike point module, the most loaded part of the divertor, measured by thermography are shown in Fig. 5. The reduction factor of the maximum heat flux in the LYRA divertor is between 2 and 3 for comparable discharge conditions.

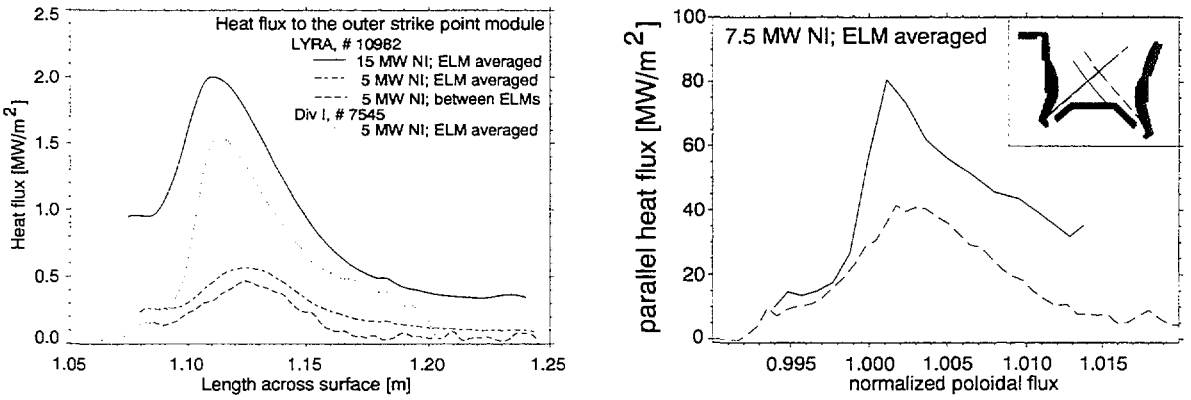

Figure 5: Heat flux to the outer strike point region measured by infrared thermography a) (left) for different discharges and b) (right) for a discharge with a strike point movement onto the roof baffle (Div I configuration). The parallel heat flux at the target is shown to eliminate geometric effects.

The ELM behaviour known from Div I, showing at the outer target plate a moderate increase of the heat flux in the ELM without changing the shape of the profile, is also found in Div II.

In addition to the variation of the plasma parameters, the strike point position was changed to check the significance of the divertor closeness and the target inclination. In one single discharge the inner and outer strike points were moved upwards by about 10 cm from a position inside the narrow divertor leg

into a region above the roof baffle. The heat flux profiles measured at the outer (vertical) target are nearly unchanged. Another discharge was used to move the outer strike point onto the (horizontal) roof baffle simulating the change from LYRA conditions to Div I situation. The maximum heat flux increased by about a factor of 2 for the roof baffle position (Fig. 5b), demonstrating the importance of the target inclination.

3.4. Radiation band between strike points and X-point

Modelling of the radiation density with the B2-Eirene code [8] predicts a small emission zone along the separatrix between the X-point and the strike points (Fig. 6a). To verify this radiation band experimentally, the plasma was moved in the z-direction, increasing the effective spatial resolution of the bolometry.

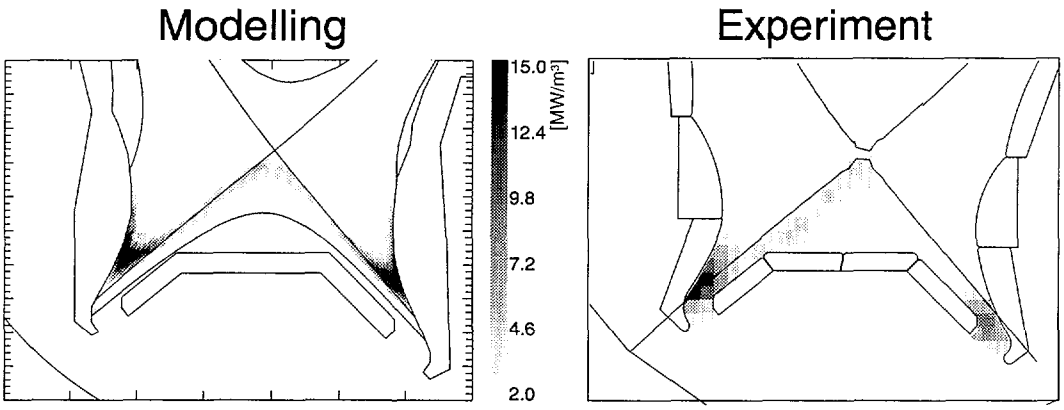

Figure 6: a) (left): B2-Eirene modelling of the radiation distribution predicts radiation bands between X-point and strike points. b) (right): Reconstructed radiation distribution using virtual lines of sight during vertical shift of the plasma reveals a narrow radiation zone from inner strike point to the X-point. A corresponding band at the outer strike point cannot be detected due to missing bolometer lines of sight.

Fig. 6b shows the ELM averaged result for a medium power (5 MW) discharge. There are two pronounced peaks of the radiation density in both the inner and outer divertor fan with values up to 15 MW/m^3. The predicted radiation band is clearly seen with a width of a few centimeters and a radiation density of about 3-4 MW/m^3 at the inner divertor. Since there are no suitable lines of sight for the outer divertor yet, the corresponding band cannot be detected there. In the main plasma one finds radiation mainly along the separatrix with radiation densities below 1 MW/m^3. Integrating the radiation density over the whole plasma, it turns out that the total radiated power is about 75% of the input power.

Measurements from various spectrometers as well as modelling with B2-Eirene show that the radiation peak directly above the strike point originates from hydrogen and carbon (C^+,C^{2+},C^{3+}), whereas only C^{2+} and C^{3+} ions contribute to the emission of the band from the strike point to the X-point.

3.5. Composition of the divertor radiation

The following analysis is aimed at separating the contribution of hydrogen and carbon to the radiative losses in Div II. For this, carbon radiation was measured for various experimental conditions (L- and H-mode, hydrogen and deuterium plasmas, heating power $P_{NI} = 1 \ldots 20$ MW) and was compared to the flux dependence of the total radiation measured by bolometry. Attached or semi-detached divertor conditions are used allowing the measurement of the particle flux rather than the density by spectroscopy.

Making use of the ion flux measured by Langmuir probes, Γ_i, and the bolometric measurements, Γ_{rad}^{bolo}, at a line of sight through the outer divertor leg a radiative potential may be estimated using the simple ansatz, $\Phi_{rad} = \frac{1}{e}\Gamma_{rad}^{bolo}/\Gamma_i$. Φ_{rad} corresponds to the total radiated energy per hydrogen ion, measured in eV (Fig. 7a), e is the elementary charge. For simplicity, it is assumed that the total radiation is caused by hydrogen and carbon so that the line of sight integrated radiative power density can be described as

$$\Gamma_{rad}^{bolo} = \Gamma_i \cdot e \cdot (\Phi_{rad}^H + Y_C \Phi_{rad}^C). \quad (1)$$

The hydrogen contribution to the total radiative potential does not depend on the particle flux and is about $\Phi_{rad}^{H} = 20$ eV. This leaves about 80 eV of carbon radiation for a hydrogen flux of $\Gamma_i = 10^{22}$ m$^{-2}s^{-1}$ (see Fig. 7a). Assuming an effective carbon erosion yield $Y_C = 2.5\%$ for this flux value, we obtain a radiative potential of carbon $\Phi_{rad}^{C} = 3.2$ keV, which is an upper estimate and includes the neglected contributions of other spurious radiators like boron and oxygen.

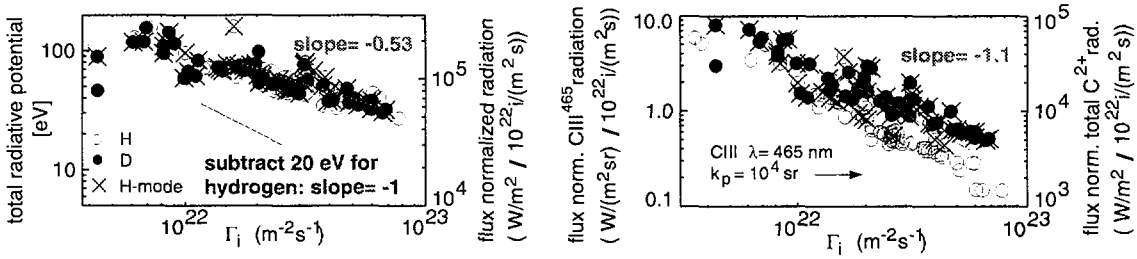

Figure 7: a) (left) Total radiative potential and line integrated power from bolometry, normalized by the ion flux, b) (right) normalized line integrated CIII (465 nm) emission.

The hydrogen-corrected total radiative potential, $\Phi_{rad}^{-H} = Y_C \Phi_{rad}^{C}$, is proportional to Γ_i^{-1} for fluxes $\Gamma_i > 10^{22}$ m$^{-2}s^{-1}$ and shows the same flux dependence as the direct CIII measurement (Fig. 7b). The flux dependence of Φ_{rad}^{-H} is mainly attributed to the flux-dependent carbon erosion yield Y_C, which has the asypmtotic dependence $Y_C \propto \Gamma_i^{-1}$ for high fluxes and adapts a flux-independent value for small values of Γ_i [9].

In order to check whether the carbon radiation estimated by bolometry can be directly reconciled by carbon spectroscopy, we calculate the C^{2+} radiative losses (predominantly in the VUV spectral range) by extrapolation of an individual line (which is accessible by spectroscopy in the visible range) using the collisional-radiative model ADAS [10]. Assuming that C^{2+} is responsible for about half of the carbon radiation (the other half originating from C^{3+}, C^{+} and C^{0}) the bolometric measurement for $\Gamma_i = 10^{22}$ m$^{-2}s^{-1}$ may be explained using realistic divertor parameters, e. g., $n_e = 3 \cdot 10^{20}$ m^{-3} and $T_e = 11$ eV. In any case, high values of the electron density are required to obtain a consistent picture of the radiated power.

3.6. Pumping and helium exhaust

Figure 8a shows compression ratios in ASDEX Upgrade, calculated from the decay rate of HeI-lines with a modified two chamber model [11]. In Div II there is some leakage from the outer pump chamber towards the main chamber with a conductance of ~70 m^3/s. This leakage and the conductance below the outer strike point module have to be taken into account in the two chamber model used previously.

The achieved compression ratios in Div II are by a factor of 2 or more higher than the values observed in Div I. Since, however, the deuterium compression ($n_{0,div}/n_{e,sep}$) is also higher, as shown in Fig. 8b, the enrichment factors (ratio of helium and deuterium compression) are in the same range as in Div I, i.e. between 0.2 and 0.5.

The higher helium compression was predicted by 2D modelling with B2-Eirene [12] and can be understood from geometric reasons. The majority of helium ions reach the divertor target not at the separatrix, but further out in the SOL. In Div I the neutrals created at the target plate had a high probability to enter the main plasma. This probability increased with their mean free path. In Div II, to the contrary, the neutrals created at the target are reflected towards the dome baffle entrance, and once they are below the dome baffle their chance of returning to the divertor plasma is rather small. To reach the dome baffle entrance, however, the neutrals have to cross the divertor leg, and here the long mean free path of helium turns into an advantage.

Therefore, from the modelling, it was also expected that helium exhaust in DIV-II would depend on the strike point position [12]. Helium neutrals, with their rather large mean free path, will enter the divertor ballistically, and the probability for doing so decreases strongly with increasing distance of the

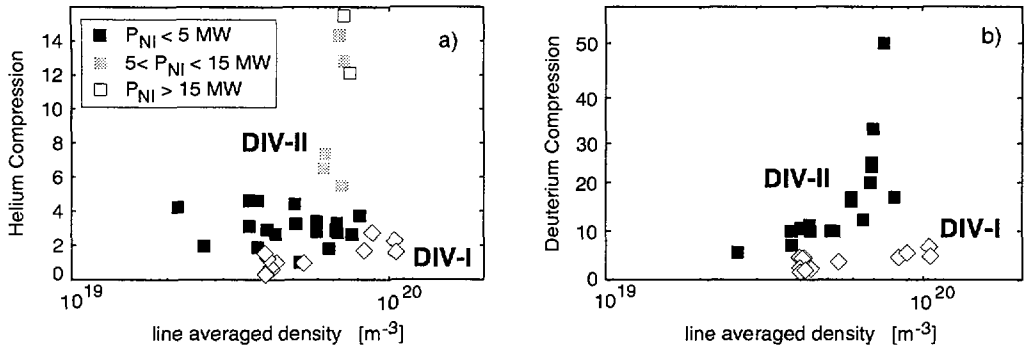

Figure 8: Helium (a) and deuterium (b) compression in ASDEX Upgrade as a function of line averaged density. Open diamonds are data from DIV I, solid squares from DIV II.

recycling location to the divertor entrance (which means a decreasing solid angle). Therefore a decrease in the He exhaust rate is expected when moving the strike point upward, while deuterium neutrals will always suffer many collisions, and they enter the divertor chamber independent of its exact location. In ASDEX Upgrade we have compared otherwise similar discharges which had either the normal strike point position or divertor strike points moved upward by 3 cm [13]. This variation did not have any influence on the deuterium compression, but the helium exhaust rate in the discharge where the strike point on the target plates is further away from the baffle entrance, is smaller by 35% in agreement with the modelling predictions. The relatively large scattering of the compression ratio, specifically at higher heating powers, may be also correlated to the preciseness of the strike point positioning.

4. DISCUSSION AND SUMMARY

In general it has been found, that the LYRA divertor with the much higher closure improves divertor performance without limiting the core plasma performance in ELMy H-mode plasmas [14]. The maximum heat flux to the LYRA divertor is reduced by more than a factor of 2 compared to Div I. The maximum heat flux measured in high power shots with a heating power up to 20 MW is below 5 MW/m^2. The reduction of the plasma heat flux in comparison to the horizontal target configuration is a result of an increased radiative power loss inside the divertor as measured by bolometry. The enhanced divertor radiation is caused by an increased combined radiation efficiency of carbon and hydrogen in the divertor plasma. Carbon cools the SOL plasma down to the 5 eV region where hydrogen losses become significant. The interplay between the following four effects seems to be the reason, which could be partly disentangled by modelling and pronounced experimental parameter variations:

- Neutrals are reflected towards the "hot" separatrix region due to the highly inclined target plates.
- The high density and an electron temperature of a few eV allow an effective radiation of hydrogen.
- Carbon produces the necessary pre-cooling of the divertor plasma to make the hydrogenic losses more effective.
- The volume for radiation is increased by broadening the SOL due to radial transport. This is especially the case for discharges with type-I ELMs as it is found experimentally [15]. Under these conditions ($P_{heat} \geq 2.5$ MW) the boundary is at the ballooning limit, resulting in an increase of $\chi_\perp$ with rising power.

B2-Eirene modelling results describe the experimental data if the carbon sputter yield and the perpendicular transport coefficient are properly adapted, and allows an insight to the physical mechanisms responsible for the increase of the divertor radiation [8].

The fact that the fractional radiative loss in the divertor is rather independent of the heating power suggests that self-regulating mechanisms are effective. For relatively cold divertor conditions, the particle flux at the target increases with power flowing into the divertor, leading to higher radiative losses. In addition, flux- and impact energy dependences of the carbon erosion may contribute to keep the divertor radiation resilient against strong variations of the input power.

Further analysis of the underlying physics processes and modelling efforts are necessary to disentangle the various effects, in combination with extensive experimental parameter variations. This is specif-

ically necessary for the extrapolation to a reactor size plasma.

Overall, the Div II results for ASDEX Upgrade demonstrate the possibility of optimizing the geometry to obtain minimum power load together with optimum particle exhaust and large operational window without negatively affecting the core confinement.

References

[1] Technical basis for the ITER final design report, cost review and safety analysis (FDR), 1997.

[2] RYTER, F. et al., Nucl. Fusion **36** (1996) 1217.

[3] BOSCH, H.-S. et al., Extension of the ASDEX Upgrade programme: Divertor II and Tungsten target plate experiment, Technical Report 1/281a, IPP, Garching, Germany, 1994.

[4] LACKNER, K., Comments Plasma Phys. Controlled Fusion **15** (1994) 359.

[5] GÜNTER, S. et al., Nucl. Fusion **38** (1998) 325.

[6] FUCHS, J. C. et al., Twodimensional reconstruction of the radiation power density in ASDEX Upgrade, in *Europhysics Conference Abstracts (Proc. of the 21th EPS Conference on Controlled Fusion and Plasma Physics, Montpellier, 1994)*, edited by JOFFRIN, E. et al., volume 18B, part III, pages 1308–1311, Geneva, 1994, EPS.

[7] HERRMANN, A. et al., J. Nucl. Mater. . (1998) to be published in Journ. Nucl. Mat.

[8] SCHNEIDER, R. et al., this conference (1998).

[9] KALLENBACH, A. et al., Nucl. Fusion **38** (1998) 1097.

[10] SUMMERS, H. P., Atomic data and analysis structure users manual, JET-IR 06 (Abingdon: JET Joint Undertaking) (1994).

[11] BOSCH, H.-S. et al., Plasma Phys. Controlled Fusion **39** (1997) 1771.

[12] SCHNEIDER, R. et al., J. Nucl. Mater. **241–243** (1997) 701.

[13] BOSCH, H.-S. et al., J. Nucl. Mater. . (1998) to be published in Journ. Nucl. Mat.

[14] BOSCH, H.-S. et al., Effect of divertor geometry on boundary and core plasma performance in ASDEX Upgrade and JET, to be published in Plasma Phys. and Contr. Fusion.

[15] HERRMANN, A. et al., Characterization of the power deposition profiles in the divertor of ASDEX Upgrade, in *Europhysics Conference Abstracts (Proc. of the 23rd EPS Conference on Controlled Fusion and Plasma Physics, Kiev, 1996)*, edited by GRESILLON, D. et al., volume 20C, part II, pages 807–810, Geneva, 1996, EPS.